PHYSICS

Experimental certification of contextuality, coherence, and dimension in a programmable universal photonic processor

Taira Giordani[1]†, Rafael Wagner[2,3]†, Chiara Esposito[1], Anita Camillini[2,3], Francesco Hoch[1], Gonzalo Carvacho[1], Ciro Pentangelo[4,5], Francesco Ceccarelli[5], Simone Piacentini[5], Andrea Crespi[4,5], Nicolò Spagnolo[1], Roberto Osellame[5], Ernesto F. Galvão[2,6]*, Fabio Sciarrino[1]*

Quantum superposition of high-dimensional states enables both computational speed-up and security in cryptographic protocols. However, the exponential complexity of tomographic processes makes certification of these properties a challenging task. In this work, we experimentally certify coherence witnesses tailored for quantum systems of increasing dimension using pairwise overlap measurements enabled by a six-mode universal photonic processor fabricated with a femtosecond laser writing technology. In particular, we show the effectiveness of the proposed coherence and dimension witnesses for qudits of dimensions up to 5. We also demonstrate advantage in a quantum interrogation task and show it is fueled by quantum contextuality. Our experimental results testify to the efficiency of this approach for the certification of quantum properties in programmable integrated photonic platforms.

INTRODUCTION

Quantum computers are capable of solving problems believed to be effectively impossible classically, such as sampling from complex probability distributions (*1*), predicting properties of physical systems (*2*), and factoring large integers (*3*). The quantum computational advantage for these tasks is built on rigorous no-go results in computational complexity theory, showing a gap between quantum and classical resources for the same task that can be exponential. Research on quantum foundations also addresses quantum advantage by asking the question: What type of quantum information processing cannot be explained classically? Answers broadly suggest a different kind of advantage, not in terms of computational power but in terms of intrinsic classical limits to information processing.

Advantage in quantum information processing pushes success rates in communication tasks (*4*–*6*), security of key distribution protocols (*7*), and success rates in discrimination tasks (*8*) beyond those that can be reached using only classical resources. This kind of advantage results from understanding quantum foundational aspects of nonclassical resources such as entanglement (*9*), coherence (*10*), Bell nonlocality (*11*), and contextuality (*12*), where classical-quantum gaps in explaining the phenomena can be predicted, bounding success rates in a quantifiable manner. For instance, phenomena that can be reproduced by noncontextual models (*13*) include interference (*14*), superdense coding (*15*), and Gaussian quantum mechanics (*16*), but it is possible to describe precisely when processing of quantum information allows an advantage over this seemingly powerful models in many tasks (*4*, *5*).

In this work, we propose and test families of coherence and contextuality witnesses in proof-of-principle device-dependent experiments carried out with single-photon states processed by a programmable integrated photonic circuit. These witnesses require the careful preparation of the system in a set of different states and then the estimation of a set of pairwise state overlaps (*17*–*20*). For this task, we encode qubits and qudits with dimensions up to five in a six-mode universal photonic processor (UPP) realized with the femtosecond laser writing technology (*21*).

We start by testing a recent quantum information advantage (*19*) for the task of quantum interrogation, first proposed as the celebrated Elitzur-Vaidman bomb-testing experiment (*22*). This task has had a profound impact in quantum foundations (*23*, *24*) that later converged into technical developments, such as the possibility of performing counterfactual quantum computation (*25*, *26*), the development of the field of quantum imaging with undetected photons (*27*, *28*), and high-efficiency interrogation using the quantum Zeno effect (*29*, *30*). We experimentally verify that the efficiency achievable by quantum theory cannot be explained by noncontextual models such as those of (*14*, *15*), as predicted in (*19*). We hence certify both the presence of this nonclassical resource in the device and its ability to use it for information processing advantage.

Although noncontextual models are capable of capturing some aspects of quantum coherence (*15*), in a way similar to how local models reproduce some aspects of quantum entanglement (*31*), coherence is still of utmost relevance for quantum information science. It plays a major role in Shor's factoring algorithm (*32*) and is crucial for the quantum advantage provided by linear-optical devices. One can then ask the question of what cannot be explained with coherence-free models. The recently established inequalities of (*17*, *20*) provide a precise answer by rigorously bounding these models.

[1]Dipartimento di Fisica, Sapienza Università di Roma, Piazzale Aldo Moro 5, I-00185 Roma, Italy. [2]International Iberian Nanotechnology Laboratory (INL), Av. Mestre José Veiga s/n, 4715-330 Braga, Portugal. [3]Centro de Física, Universidade do Minho, Campus de Gualtar, 4710-057 Braga, Portugal. [4]Dipartimento di Fisica, Politecnico di Milano, Piazza Leonardo da Vinci, 32, I-20133 Milano, Italy. [5]Istituto di Fotonica e Nanotecnologie, Consiglio Nazionale delle Ricerche (IFN-CNR), Piazza Leonardo da Vinci, 32, I-20133 Milano, Italy. [6]Instituto de Física, Universidade Federal Fluminense, Av. Gal. Milton Tavares de Souza s/n, Niterói, RJ, 24210-340, Brazil.
*Corresponding author. Email: ernesto.galvao@inl.int (E.G.); fabio.sciarrino@uniroma1.it (F.S.)
†These authors contributed equally to this work.

We show theoretically, numerically, and experimentally that a family of inequalities introduced in (*19*) has a particularly interesting property: Violations of these inequalities witness not only coherence inside the interferometers but also the dimensionality of the information encoded. Since Hilbert space dimension is itself a resource, the question of what can be done only with qudits is of relevance for information processing. Some information tasks do require qudits (*33*–*36*) or have their security linked to the dimension (*37*), so an important research field is devoted to developing methods to guarantee lower bounds on the Hilbert space dimension attained by different physical systems (*38*–*42*).

The fact that this family of inequalities has violations only for coherent qudits marks a new paradigm for quantum coherence allowed by the basis-independent perspective (*17*, *43*). There exists quantum coherence that is achieved by qudits that cannot be achieved with qubits. Such a fact has no precedent from the resource theoretic perspective of basis-dependent coherence (*10*). Coherence captured only with qudits was first considered in (*44*). We experimentally witness this proposed new form of coherence for qutrits, ququarts, and ququints inside a six-mode programmable integrated UPP. We prove that the inequality violated by pure qutrits cannot be violated by qubits, complementing this result with numerical and experimental investigations, and we perform a similar analysis for our inequalities violated by ququart and ququint systems. In doing so, we extend the dimension witness result from (*18*) both qualitatively and quantitatively, making the best use of the flexibility and accuracy of our multimode processor.

RESULTS

Theoretical framework

Quantum coherence is commonly described as a basis-dependent property. Given some space $\mathcal{H}$ describing a system and a fixed basis $\Omega = \{|\omega\rangle\}_\omega$, any state ρ is said to be coherent if it is not diagonal with respect to Ω. It is possible to avoid basis dependence by considering sets of states (*43*). Given any set of states $\underline{\rho} = \{\rho_i\}_{i=0}^{n-1}$, the entire set is said to be basis-independent coherent, or simply set coherent, if there exists no unitary U such that $\underline{\rho} \mapsto \underline{\sigma} = \underline{U\rho U^\dagger} = \{U\rho_i U^\dagger\}_{i=0}^{n-1}$, with every $\sigma_i = U\rho_i U^\dagger$ diagonal.

Witnesses of such a notion of basis-independent coherence were proposed in (*17*), building on the realization that set coherence is a relational property among the states in $\underline{\rho}$. Bargmann invariants (*45*, *46*) completely characterize all the relational information of any set of states. The simplest such invariants are the two-state overlaps $r_{i,j} = \mathrm{Tr}(\rho_i\rho_j)$, for $\rho_i, \rho_j \in \underline{\rho}$. In Methods and note S1, we recall why the overlap inequalities of (*17*, *20*) serve as set coherence witnesses. The first nontrivial inequality bounding coherence [Galv 17] was experimentally investigated in (*18*) and bounds the three overlaps of a set of three states

$$r_{0,1} + r_{0,2} - r_{1,2} \leq 1 \tag{1}$$

Violations of these inequalities represent witnesses of basis-independent coherence of $\underline{\rho} = \{\rho_i\}_{i=0}^{2}$. However, as was shown in (*20*), this is also a witness of contextuality when we interpret each state either as an operational preparation procedure or as a measurement effect. In note S2, we review in detail how these inequalities help to characterize contextuality.

As part of our certification, we perform a quantum information task known as (standard) quantum interrogation (*22*) that can be performed using a two-mode Mach-Zehnder interferometer (MZI) setup, as depicted in Fig. 1A, and interpreted in light of our discussion about the connection between coherence and contextuality. For the purpose of testing our device, we will quantify the success rate of the interrogation task using the efficiency η given by

$$\eta = \frac{p_{\mathrm{succ}}}{p_{\mathrm{succ}} + p_{\mathrm{abs}}} \tag{2}$$

where p_{succ} is the probability of successfully detecting the presence of the object without it absorbing the photon and p_{abs} corresponds to the probability of absorption. In Methods, we precisely describe the task, and how these probabilities relate to the MZI beam-splitting ratio. Wagner *et al.* (*19*) showed that noncontextual models cannot explain η for arbitrary beam-splitting ratios and that there exists a quantifiable gap between the efficiencies achievable by quantum theory and noncontextual models. We provide a more robust discussion of this result in notes S2 to S4, where we model the noise resistance of the contextual advantage result, describing also related loopholes for testing contextuality of the obtained data. In the remaining of the certification, we will solely focus on nonclassicality provided by set coherence.

Violations of the inequalities of (*19*) are a promising, scalable, and efficient way to witness coherence inside multimode interferometers, as described in Fig. 1B (see also note S1). A multipath interferometer corresponds to an efficient device for generating high-dimensional coherent states and measuring their two-state overlaps.

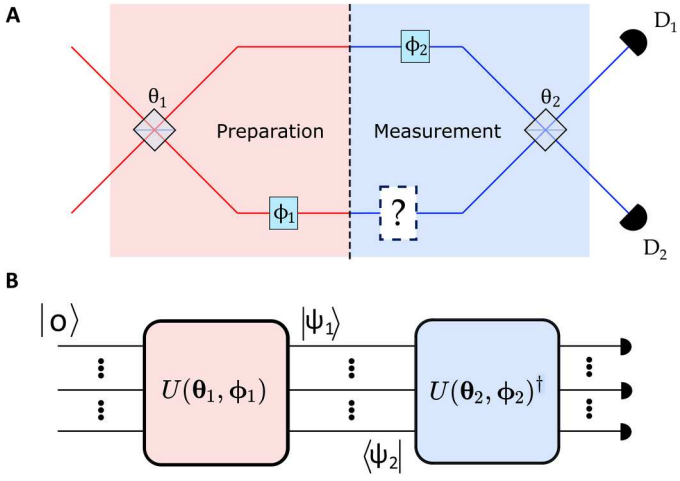

Fig. 1. MZI and its multimode generalization for quantum interrogation, coherence, and dimension witnesses. (**A**) Any MZI can be ideally separated in a preparation stage (red), in which we prepare a qubit state $\psi(\theta_1, \phi_1)$ and a measurement stage (blue) that projects onto another qubit state $\psi(\theta_2, \phi_2)$. In a quantum interrogation experiment, the ? box is an object that absorbs photons. (**B**) In analogy with the MZI, a multipath interferometer encodes *d*-level systems by a set of beam splitters $\boldsymbol{\theta}_1$ and phase shifters $\boldsymbol{\phi}_1$ that operate on the *d* mode as a unitary operator $U(\boldsymbol{\theta}_1, \boldsymbol{\phi}_1)$. In the second stage, another round of beam splitters $\boldsymbol{\theta}_2$ and phase shifters $\boldsymbol{\phi}_2$ followed by a series of photodetectors detects photons at the *d* output ports. With a single-photon input at the top input mode 0, this setup is capable of measuring two-state overlaps $|\langle\psi_2|\psi_1\rangle|^2 = |\langle 0|U(\boldsymbol{\theta}_2, \boldsymbol{\phi}_2)^\dagger U(\boldsymbol{\theta}_1, \boldsymbol{\phi}_1)|0\rangle|^2$.

Consider any two states, $|\psi_1\rangle = U(\boldsymbol{\theta}_1, \boldsymbol{\phi}_1)|0\rangle$ and $|\psi_2\rangle = U(\boldsymbol{\theta}_2, \boldsymbol{\phi}_2)|0\rangle$, over some finite-dimensional Hilbert space in which 0 is one state of a given basis. Their overlap can be measured choosing the two stages of a generic interferometer such that

$$r_{1,2} \equiv r_{2,1} = |\langle\psi_2|\psi_1\rangle|^2 = |\langle 0|\, U(\boldsymbol{\theta}_2, \boldsymbol{\phi}_2)^{\dagger} U(\boldsymbol{\theta}_1, \boldsymbol{\phi}_1)|\, 0\rangle|^2 \quad (3)$$

Using multimode devices, it is possible to witness not only coherence but coherence achievable only with qudits by violation of the following family of inequalities defined recursively

$$h_n(r) = h_{n-1}(r) + r_{0,n-1} - \sum_{i=1}^{n-2} r_{i,n-1} \leq 1 \quad (4)$$

where the sequence starts with $h_3(r) = r_{0,1} + r_{0,2} - r_{1,2}$ and the above equation defines inequalities for any integer $n > 3$. When $n = 4$, we have

$$h_4(r) = r_{0,1} + r_{0,2} + r_{0,3} - r_{1,2} - r_{1,3} - r_{2,3} \leq 1 \quad (5)$$

The inequality in Eq. 5 cannot be violated by a set of pure qubit states. With qutrits, it reaches violations up to 1/3. Hence, quantum violations of inequality (5) represent witnesses of both coherence and Hilbert space dimension higher than 2. We have numerically found the same behavior for sets of pure quantum states for the family of h_n inequalities (4) up to h_{10} by maximizing over parameters describing up to 10 states. This is evidence that the family of inequalities (4) corresponds to simultaneous witnesses of coherence and dimension, achievable only by the device's capability of precisely preparing and measuring high-dimensional coherent states. We do not prove that these inequalities have this property for all values of n. Using semidefinite programming (SDP) techniques, we show that we can map the maximum possible values of the inequalities (4) to the solutions of a quadratic SDP. We then show that, for n up to $n = 2^{12}$, sets of states with dimension $d = n - 1$ are capable of violating the inequalities h_n, while no violation is obtained from states spanned by a basis of any lower dimension. In note S1, we present these theoretical results and discuss the underlying assumptions for the dimensionality certification in detail.

Experimental implementation and results

Quantum interrogation and coherence witnesses are tested in heralded single-photon experiments, by means of the experimental setup shown in Fig. 2, composed of a single-photon source based on parametric down-conversion and a programmable integrated UPP fabricated via femtosecond laser micromachining (see Methods for more details). Let us now discuss the results obtained in the performed experiments.

Coherence and contextuality in two-level systems

In the previous section, we have provided the theoretical framework that derives families of coherence witnesses based on the evaluation of pairwise overlaps among states in a finite set. Some inequalities tailored to work as coherence witnesses can also witness quantum contextuality. We have already mentioned inequality (1) as one of such example. Furthermore, this inequality predicts an advantage for the efficiency in the task of quantum interrogation (*19*). We implement and test this task in a programmable MZI inside the integrated UPP. The experimental optical circuit is shown Fig. 3A. In our experiment, the absorbing object is modeled by a completely transparent beam splitter with reflectivity $r_B = \sin\theta_B = 0$ placed in one arm of the MZI. The MZI is calibrated so that the two beam splitters have the same beam-splitting ratio ($\theta_1 = \theta_2 = \theta$), with a null internal phase ($\phi = 0$). These conditions guarantee that a single photon injected in mode 0 will always come out of output 0 when the object is absent. The aim of this experiment is to estimate the efficiency η of detecting the presence of the object without it absorbing the photon, as defined in Eq. 2. In our scheme, p_{succ} corresponds to the fraction of single photons detected in mode 1, since this output is only possible when the object is present. The probability of absorption p_{abs} is given by the fraction of photons detected in mode 2. In Fig. 3B, we report the measurements of η for different values of the reflectivity $r = \sin\theta$ of the two beam splitters. The theoretical curve is given by a quantum model of the MZI, whose performance is, in general, not achievable by any generalized noncontextual model (see also note S2), given by

$$\eta = \frac{r(1-r)}{r(1-r) - r + 1} \quad (6)$$

Our experimental data follows very well the predictions of the quantum model, showing not only that the device generates data that cannot be explained with noncontextual models but also that it uses contextuality as a resource to achieve quantum-over-classical performance, quantified by the efficiency η. We observe that the largest deviations from the theoretical curve appear for values of r close to 1. This discrepancy can be justified by taking into account the experimental imperfections in the apparatus (see Methods).

In notes S2 to S4, we present a detailed discussion about contextuality in MZIs, including an analysis of the requirements for witnessing contextuality when the device is used for the quantum interrogation task. In there, we pick a specific beam splitter configuration for the interrogation task and show that we experimentally achieve $\eta_{\text{exp}} = 0.428 \pm 0.006$, while noncontextual models must have an efficiency $\eta^{\text{NC}} \leq 0.410$ even when benefiting from the effect of noise, which raises the noncontextual upper bound for η.

In note S5, we also certify coherence in the MZI using a different and previously unidentified inequality featuring a high level of violation by five symmetrical states on a great circle of the Bloch sphere.

Coherence and dimension witnesses in higher dimensions

Equation 4 describes a family of inequalities that are tailored for certifying coherence in systems with dimension $d > 2$. We will refer to these inequalities as h_n, where n is the number of states in the set whose overlaps we need to evaluate. They arise as inequalities obtained using the event graph approach (*20*), when we consider complete graphs K_n. The presence of coherence in the states is witnessed when an inequality is violated, that is, when $h_n > 1$. An important point to note is that the values $h_n(r)$ provide information regarding the coherence accessible only due to the dimension of the space. The h_n inequalities are not violated by sets of states without coherence nor by systems with dimension $d < n - 1$. For example, one-qubit states do not violate $h_4 \leq 1$, qutrit states do not violate $h_5 \leq 1$, and so on.

The main result is that h_n displays different maximum values according to the dimension of the system. This implies that the functionals $h_n(r)$ are not only dimension witnesses but also indicators of the dimension of the space.

We tested firstly the effectiveness of h_4, h_5, and h_6 inequalities as coherence witnesses. In Fig. 4, we show the circuits to prepare and measure three-, four-, and five-mode qudits. In particular, the red

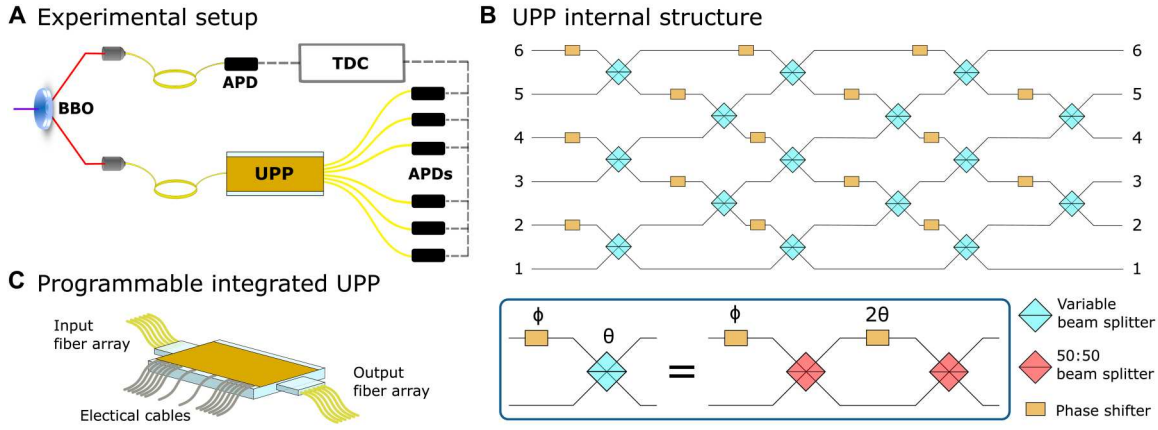

Fig. 2. Experimental setup and UPP. (**A**) Experimental setup. A pair of photons is generated by a spontaneous parametric down conversion (SPDC) source. One photon is detected as trigger. The second photon is sent in a programmable integrated UPP that can realize a generic unitary transformation. At the output of the chip, we measure the twofold coincidence between the photon in the chip and the trigger photon. They are detected by exploiting avalanche photo-diode detectors (APDs). (**B**) UPP internal structure. The optical circuit is a six-mode rectangular mesh of variable beam splitters and phase shifters, enabling the implementation of arbitrary 6×6 unitary transformations. Each variable beam splitter is actually a MZI structure with two 50:50 beam splitters and a phase shifter in between (see the inset). (**C**) Programmable integrated UPP. The integrated device used in the experiment is a UPP, realized by the femtosecond laser writing technique in an alumino-borosilicate glass substrate. Two fiber arrays are directly plugged in at the input and at the output of the interferometer. Thermo-optic phase shifters are patterned with the same technology on a thin gold layer deposited on the substrate. Electrical currents are supplied to the phase shifters through interposing printed circuit boards (not shown in figure for the sake of simplicity), allowing one to locally heat the waveguides and change the settings of the optical device. BBO, beta-barium borate crystal; TDC, time-to-digital converter.

part of the circuits for qutrit (Fig. 4A) and ququart (Fig. 4B) is universal state preparators when a single photon enters the device respectively in inputs 0 and 1. In the case of five-mode qudits, the six-mode UPP does not have enough layers of MZIs to implement independent universal preparation and measurement stations. However, the circuit in Fig. 4C can prepare a set of six five-mode qudit states that maximize h_6. In the figure, we also report the h_n values together with the matrix of the pairwise overlaps. We estimated the violations by considering only the upper triangular part of such a matrix, i.e., $r_{i,j}$, with $i > j$. Further details on the sets of states used to violate the inequalities and a discussion on the sources of noise in the experimental measurements are reported in notes S6 and S7.

We then move to the experimental test of h_n as dimension witnesses by sampling uniformly random states spanned by bases of different dimensions. The distributions of the values obtained for the left-hand side of the h_n inequalities for $d = 2$, $d = 3$, and $d = 4$ are reported in Fig. 5, together with the maximum theoretical values of h_n for systems of those dimensions. The experimental data confirm the theoretical predictions. This provides further insight on the power of the h_n as dimension witnesses. The uniform sampling of the states tries to answer the following question: How much information about the dimension of the space can we retrieve from the value of the left-hand side of the h_n inequalities, without knowing the optimal set that maximizes the violation? We did not sample random states in $d = 5$ because our circuits are not universal state preparators and measurement devices for qudits of this dimension. Table 1 summarizes the maximum values of the functionals h_n obtained in the random sampling and in the previous analysis dedicated to coherence witnesses. We see that the maximum violations are not typically achievable when sampling random states. However, the h_n become very effective in discerning systems of $d > 2$ for increasing values of n.

In summary, we showed how to exploit new families of overlap inequalities to witness coherence in qudit systems. The coherence is certified when $h_n > 1$. Furthermore, the h_n inequalities introduced in (*20*) and tested here are only violated by systems having both coherence and a dimension $d \geq n - 1$. Even when $h_n < 1$, while not witnessing coherence, the value of h_n still provides information on the dimension.

DISCUSSION

In this work, we have characterized how quantum information is processed within a six-mode programmable integrated UPP. To do so, we witnessed—and used—two different notions of quantum nonclassicality, namely, generalized contextuality and coherence. Our characterization of nonclassicality is done in a way that depends on the dimension of the Hilbert space generated by single-photon interference through the paths of the programmable device. Our analysis begins with the simplest scenario, where we use a subsection of the device to implement a two-mode MZI. We demonstrate the presence of generalized contextuality within the MZI by violation of a recently introduced generalized noncontextuality inequality. We show that this resource is used to achieve efficiencies in the task of quantum interrogation that are higher than those possible by any noncontextual model that reproduces the same operational constraints considered in our experiment.

Then, we proceeded to investigate nonclassicality generated by a single photon able to propagate through gradually larger portions of the interferometer. In doing so, we introduce a previously uninvestigated theoretical perspective in coherence theory: quantum coherence achievable only by qudits. We show that a family of inequalities is capable of identifying coherence that can only be witnessed when the totality of the Hilbert space dimension considered is used in nontrivial ways. We experimentally measure the presence of this

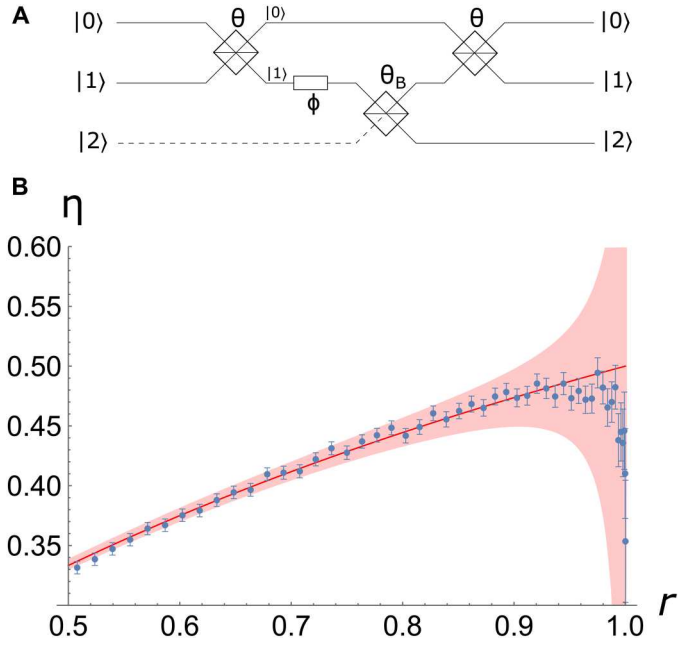

Fig. 3. Coherence and contextuality in a MZI. (**A**) Scheme of the circuit used for the quantum interrogation task. (**B**) Efficiency η of the object's detection versus the reflectivity $r = \sin\theta$ of the two beam splitters in the MZI. The red curve is the theoretical prediction, while the red shaded area represents the deviations from the ideal model due to dark counts and imperfect calibration of the beam splitters. The error bars derive from the poissonian statistics of the single-photon counts.

kind of coherence for a single photon interfering in up to five modes. Via numerical simulations, we demonstrate that this family of inequalities is a simultaneous witness of coherence and Hilbert space dimension d up to $d = 2^{12}$.

Our certification scheme leaves some opportunities for further theoretical investigation. For instance, while our scheme is not device independent, we believe that in the future it may be suitable for a description in the semi-device independent framework, since our single requirement over the data is that it corresponds to two-

Table 1. Experimental results for witnesses of coherence and dimension. In bold are the h_n values that we measured for the coherence witnesses, and in roman are the maximum experimental values measured in the uniform random sampling of ~200 sets of states of dimension d.

	$d = 2$	$d = 3$	$d = 4$	$d = 5$
h_4	1.05 ± 0.01	**1.31 ± 0.01**	1.23 ± 0.01	
h_5	0.36 ± 0.02	0.84 ± 0.02	**1.39 ± 0.01**	
h_6	−0.96 ± 0.04	0.17 ± 0.03	0.40 ± 0.02	**1.38 ± 0.01**

state overlaps, possibly interpreted as a promise over the possible measurements. Quantum states, Hilbert spaces and physical devices are arbitrary. Also, because of the invariant properties of the inequalities, their maximization will likely be related to the task of self-testing (*47*), and techniques used there might be applicable in our case.

We believe that violation of these inequalities can be exploited in the future as an effective certification technique benchmarking nontrivial high-dimensional coherence and that may be related to hardness of quantum computation. Moreover, the theoretical results presented here apply to any platform for quantum computation and not just photonics.

METHODS

Experimental setup

A BBO crystal is pumped by a pulsed laser at the wavelength of λ = 392.5 nm. The spontaneous parametric down conversion process generates photon pairs at λ = 785 nm. In the experiment, we focus on one pair emissions, much more likely to happen than multipair generation.

One of the two photons is used as a trigger signal, while the other one is injected in a UPP, i.e., a fully programmable multimode interferometer. This device consists in a waveguide circuit, fabricated in-house by the femtosecond laser writing technology in an

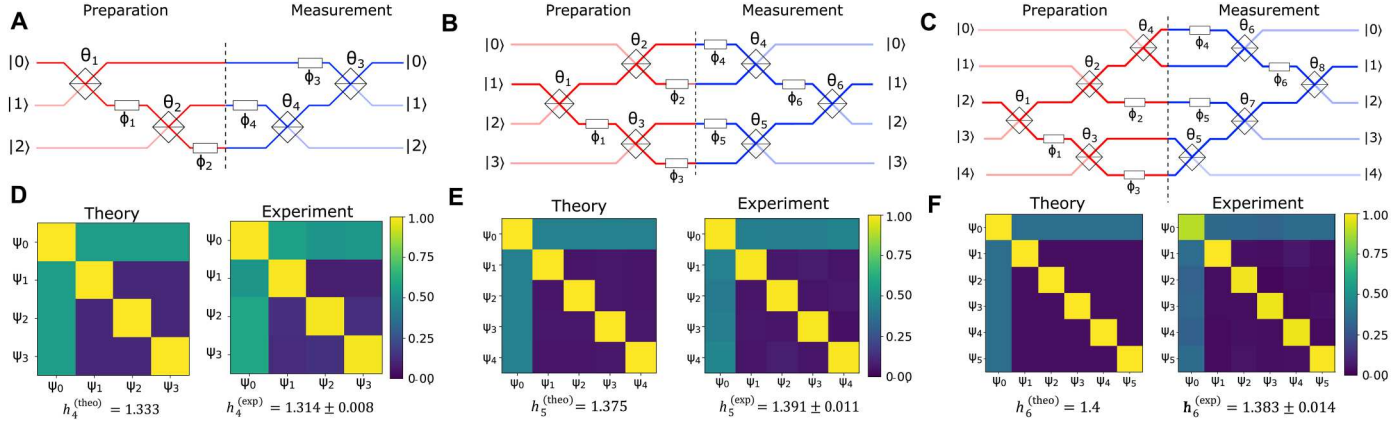

Fig. 4. Violations of h_n inequalities by qudits. (**A** to **C**) Circuit schemes for qutrits (A), ququarts (B), and five-mode qudits (C) preparation (red part) and measurement (blue). The single-photon signal enters from mode 0 for the qutrits case, from mode 1 for ququarts, and from mode 2 for the five-mode case. (**D** to **F**) Comparison of the theoretical and the experimental matrices of the pairwise overlaps values $r_{i,j} = |\langle\psi_j | \psi_i\rangle|^2$ for the sets of states that maximize the violation of h_4, h_5, and h_6. In particular, h_4 is violated by sets of four qutrit states $\{\psi_0, \ldots\psi_3\}$ in (D), the h_5 inequality is violated by sets of five ququart states $\{\psi_0, \ldots, \psi_4\}$ in (E), and h_6 is violated by sets of six quantum states of dimension 5 $\{\psi_0, \ldots, \psi_5\}$ in (F). The uncertainty reported for each inequality derives from the poissonian statistics of the single-photon counts.

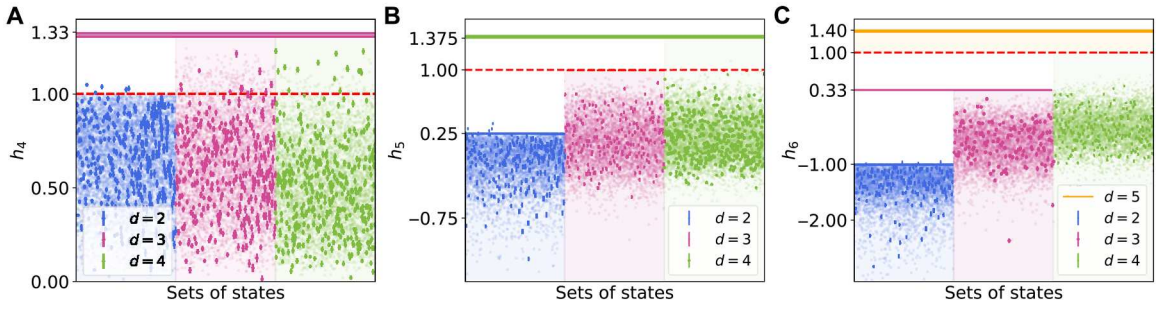

Fig. 5. h_n inequalities as dimension witnesses. Random states sampled uniformly in Hilbert spaces of dimensions 2 (blue), 3 (purple), and 4 (green). Bold points correspond to ∼200 experimental preparations of sets of uniformly random qudit states for each dimension. The uncertainties are smaller than the points' size. The shaded points in the background are ∼5000 sets of numerically simulated states for each dimension. The dotted red line indicates the threshold value 1 for h_n required to witness coherence. (**A**) Distributions of the $h_4(r)$ values. The purple line is the maximum violation of the h_4 inequality for state dimension $d = 3$. (**B**) Same analysis for the h_5 inequalities. Here, we observe a lower bound for $d = 2$, highlighted by the blue line, that allows better discrimination of high-dimensional sets of states. The green line is the maximum violation achieved with the set that includes states of $d = 4$. (**C**) Distributions for the h_6 inequality. We report only the maximum violation measured for the coherence witness because our setup is not a universal state preparator for $d = 5$. Blue and purple lines highlight the maximum values of h_6 for $d = 2$ and $d = 3$, respectively.

alumino-borosilicate glass chip. The scheme of the photonic circuit of the six-mode UPP is reported in Fig. 2C and follows the decomposition into a rectangular network of beam splitters and phase shifters devised in (*48*). The beam splitters in the scheme are actually MZIs (see inset in Fig. 2C), which provide variable splitting ratios depending on the value of the internal phase. The dynamic reconfiguration of the UPP operation is accomplished by thermo-optic phase shifters, which enable the active control of the values of the phase terms placed inside and outside the cascaded MZIs. The input and output ports of the waveguide circuit are optically connected via fiber arrays (single mode fibers at the input and multimode fibers at the output, see also Fig. 2B).

In particular, the phase shifters are based on gold microheaters, deposited and patterned on the chip surface. Upon driving suitable currents into the microheaters, local heating of the substrate is achieved in a precise and controlled way. This local heating induces, in turn, a refractive index change and thus controlled phase delays in the waveguides due to the thermo-optic effect. A careful calibration of the phase shifters allows to implement with our UPP any linear unitary transformation of the input optical modes. This calibration is performed by classical coherent light and does not rely on the quantum theory we test in our experiments. More details on the design, fabrication and calibration process of the UPP are provided in note S8.

Last, the outputs and the trigger photon fibers are connected to avalanche-photodiode single-photon detectors. The detector signals are processed by a time-to-digital converter that counts the twofold coincidence between the chip outputs and the trigger photon.

Noise model for the quantum interrogation experiment

The main sources of noise that need to be considered for the quantum interrogation experiment are mismatches in the reflectivity r of the two beam splitters and dark counts of the detectors. These become more significant for $r \sim 1$, since in this regime, both p_{succ} and p_{abs} tend to be very small. Our noise-corrected formula for η will be

$$\eta_{\mathrm{noisy}} = \frac{r[1-(1\pm\varepsilon)r]+n_1}{r[1-(1\pm\varepsilon)r]-r+1+n_1+n_2} \tag{7}$$

where ε is the percentage mismatch of the two reflectivities and n_1 and n_2 indicate the ratio between dark counts and signal.

The red area in Fig. 3B encloses the set of curves resulting from a span of the parameters ε, n_1, and n_2 in the range 0 and 0.005. Our noise model predicts large deviations from the ideal quantum efficiency when the beam-splitting ratio approaches $r = 1$.

Pairwise overlap inequalities characterizing incoherent sets of states

We will briefly recall the arguments from (*17*, *19*) for why the selected inequalities are capable of bounding the overlaps of sets of incoherent states, and how a graph-theoretic construction enables finding these inequalities.

For a diagonal set of states, with respect to any basis, the two-state overlaps $\mathrm{Tr}(\rho_i\rho_j)$ of the elements $\{\rho_i\}_i$ of that set represent the probability of obtaining equal outcomes from the states upon measurements with respect to the reference basis. When such an interpretation is possible, we say that the set of states is coherence-free, or incoherent, and the reference basis is a coherence-free model for this set. For each set of states $\underline{\rho}$, it is possible to define an edge-weighted graph (G, r) with vertices of the graph $V(G)$ representing quantum states and edges $E(G)$ having weights $r_e \equiv r_{i,j} \coloneqq \mathrm{Tr}(\rho_i\rho_j)$. If we collect all weights into a tuple $r = (r_e)_e \in \mathbb{R}^{|E(G)|}$ with $|E(G)|$, the total number of edges in the (finite) graph G, it is possible to bound all tuples r, resulting from states that are diagonal with respect to some basis. This was studied in (*17*, *20*), and the bounds are given by linear inequalities. Similar to what is already well established in Bell nonlocality (*11*) and contextuality (*12*), inequalities bound descriptions of classicality; those inequalities are built to bound coherence-free models for $\underline{\rho}$.

The basic reasoning described in its most general form starts by acknowledging that, if all states are incoherent, there exists some set of output outcomes Ω with respect to which the weights $r_{i,j}$ represent the probability that, upon independently measuring ρ_i, ρ_j from adjacent nodes i, j in the graph G, we obtain equal outcomes. As an example, consider two adjacent nodes described by the maximally

mixed qubit state $I_2/2$. In this case, the edge-weight corresponds to the two-state overlap $\mathrm{Tr}(I_2/4) = 1/2$. This is also the probability that we measure these two states with respect to the basis that diagonalizes them and obtain equal outcomes, i.e., the probability that two ideal coins return equal outcomes.

To find overlap inequalities the algorithm then goes as follows: for a given graph G we have all conceivable tuples $r = (r_e)_e$ described by all assignments 0 or 1. Any tuple of two-state overlaps will be inside the polytope described by the hypercube $[0,1]^{|E(G)|}$. Using the assumption of incoherent states and what this forces overlaps to satisfy, i.e., to be the probability of equal outcomes with respect to some set of labels, one can forbid some assignments from the hypercube. The remaining ones are just those possible from an incoherent interpretation of states and edge-weights. In convex geometry, the convex hull of this set of assignments defines a polytope, and using standard tools it is possible to find the facet-defining inequalities for this polytope, given that the vertices are known. These facet-defining inequalities are the inequalities we probe in our work. By construction, inequality violations immediately contradict the hypothesis of incoherent states, hence serving as witnesses of set-coherence.

In this work, the graphs considered are only complete graphs K_n, a graph where every is connected to every other node, for $n = 3, 4, 5, 6$. The label n describes the number of nodes for the graph. The inequalities described by Eq. 4 form one among many inequalities that can be derived for the graph K_n, having the particularly interesting properties we discuss in the main text. In the Supplementary Materials, we describe a different inequality from the same graph that has a large violation that can be violated with qubits. For a more detailed description, we refer to (*20*).

Standard quantum interrogation task

For the interrogation task, one assumes that there might be some object in one of the interferometer′s arms, depicted as a question mark in Fig. 1A. The object, if present, is assumed to completely absorb incoming photons, and the task is to detect the presence of the object without any photons being absorbed by the object. It is somewhat unexpected that such a task can be accomplished at all, but using the fact that beam splitters create coherence, a simple set-up is capable of performing the task. Letting two 50:50 beam splitters and no difference in phase between the arms, in case there is no object, all the coherence created in the preparation stage is destroyed in the measurement stage, and one of the detectors never lights up. However, in the presence of an object, it acts as a complete path-information measurement device inside the interferometer, projecting the state of the photon inside the interferometer to the arm where the object is not present. This happens with 50% probability. When the nonabsorbed photon hits the second beam splitter in the measurement stage, there is a 50% chance that the detector that would be dark in the absence of an object now lights up. Therefore, with probability 25%, one can detect the presence of the object without directly interacting with it. Unexpectedly, there are noncontextual models capable of reproducing precisely this feature (*14*).

We can vary the beam-splitting ratios for the protocol, which allows us to have an improvement in the efficiency of the task. It is crucial that the second beam splitter in the MZI perfectly reverses the first beam splitter′s action, so that whenever we have no object inside the interferometer, or we have an inactive object, one of the detectors never clicks (remaining dark). The probabilities p_{succ} and p_{abs} depend on the beam-splitting ratio characterizing the beam splitter. The probability p_{abs} is simply the probability that once the photon enters the device, it goes to the arm that has the object. The probability p_{succ} is the probability that the photon does not reach the object, hence going to the other arm, and leaves the MZI via the output port that is dark in the absence of the object.

Supplementary Materials

This PDF file includes:

Notes S1 to S8
Figs. S1 to S9
Tables S1 and S2
References

REFERENCES AND NOTES

1. S. Aaronson, A. Arkhipov, The computational complexity of linear optics, in *Proceedings of the 43rd annual ACM symposium on Theory of computing* (ACM Press, 2011).
2. H.-Y. Huang, R. Kueng, J. Preskill, Predicting many properties of a quantum system from very few measurements. *Nat. Phys.* **16**, 1050–1057 (2020).
3. P. W. Shor, Polynomial-time algorithms for prime factorization and discrete logarithms on a quantum computer. *SIAM Rev.* **41**, 303–332 (1999).
4. D. Saha, A. Chaturvedi, Preparation contextuality as an essential feature underlying quantum communication advantage. *Phys. Rev. A* **100**, 022108 (2019).
5. R. W. Spekkens, D. H. Buzacott, A. J. Keehn, B. Toner, G. J. Pryde, Preparation Contextuality Powers Parity-Oblivious Multiplexing. *Phys. Rev. Lett.* **102**, 010401 (2009).
6. H. Buhrman, R. Cleve, S. Massar, R. de Wolf, Nonlocality and communication complexity. *Rev. Mod. Phys.* **82**, 665–698 (2010).
7. A. K. Ekert, Quantum cryptography and bell's theorem, *in Quantum Measurements in Optics* (Springer, 1992), pp. 413–418.
8. D. Schmid, R. W. Spekkens, Contextual advantage for state discrimination. *Phys. Rev. X* **8**, 011015 (2018).
9. R. Horodecki, P. Horodecki, M. Horodecki, K. Horodecki, Quantum entanglement. *Rev. Mod. Phys.* **81**, 865–942 (2009).
10. A. Streltsov, G. Adesso, M. B. Plenio, *Colloquium*: Quantum coherence as a resource. *Rev. Mod. Phys.* **89**, 041003 (2017).
11. N. Brunner, D. Cavalcanti, S. Pironio, V. Scarani, S. Wehner, Bell nonlocality. *Rev. Mod. Phys.* **86**, 419–478 (2014).
12. C. Budroni, A. Cabello, O. Gühne, M. Kleinmann, J.-A. Larsson, Kochen-Specker contextuality. *Rev. Mod. Phys.* **94**, 045007 (2022).
13. R. W. Spekkens, Contextuality for preparations, transformations, and unsharp measurements. *Phys. Rev. A* **71**, 052108 (2005).
14. L. Catani, M. Leifer, D. Schmid, R. W. Spekkens, Why interference phenomena do not capture the essence of quantum theory. *Quantum* **7**, 1119 (2023).
15. R. W. Spekkens, Evidence for the epistemic view of quantum states: A toy theory. *Phys. Rev. A* **75**, 032110 (2007).
16. S. D. Bartlett, T. Rudolph, R. W. Spekkens, Reconstruction of Gaussian quantum mechanics from Liouville mechanics with an epistemic restriction. *Phys. Rev. A* **86**, 012103 (2012).
17. E. F. Galvão, D. J. Brod, Quantum and classical bounds for two-state overlaps. *Phys. Rev. A* **101**, 062110 (2020).
18. T. Giordani, C. Esposito, F. Hoch, G. Carvacho, D. J. Brod, E. F. Galvão, N. Spagnolo, F. Sciarrino, Witnesses of coherence and dimension from multiphoton indistinguishability tests. *Phys. Rev. Res* **3**, 023031 (2021).
19. R. Wagner, A. Camillini, E. F. Galvão, Coherence and contextuality in a Mach-Zehnder interferometer. arXiv:2210.05624 [quant-ph] (11 Ocotber 2022).
20. R. Wagner, R. S. Barbosa, E. F. Galvão, Inequalities witnessing coherence, nonlocality, and contextuality. arXiv:2209.02670 [quant-ph] (6 September 2022).
21. G. Corrielli, A. Crespi, R. Osellame, Femtosecond laser micromachining for integrated quantum photonics. *Nanophotonics* **10**, 3789–3812 (2021).
22. A. C. Elitzur, L. Vaidman, Quantum mechanical interaction-free measurements. *Found. Phys.* **23**, 987–997 (1993).
23. L. Vaidman, The Meaning of the Interaction-Free Measurements. *Found. Phys.* **33**, 491–510 (2003).

24. L. Hardy, On the existence of empty waves in quantum theory. *Phys. Lett. A* **167**, 11–16 (1992).
25. O. Hosten, M. T. Rakher, J. T. Barreiro, N. A. Peters, P. G. Kwiat, Counterfactual quantum computation through quantum interrogation. *Nature* **439**, 949–952 (2006).
26. Y. Liu, L. Ju, X.-L. Liang, S.-B. Tang, G.-L. S. Tu, L. Zhou, C.-Z. Peng, K. Chen, T.-Y. Chen, Z.-B. Chen, J.-W. Pan, Experimental Demonstration of Counterfactual Quantum Communication. *Phys. Rev. Lett.* **109**, 030501 (2012).
27. G. B. Lemos, V. Borish, G. D. Cole, S. Ramelow, R. Lapkiewicz, A. Zeilinger, Quantum imaging with undetected photons. *Nature* **512**, 409–412 (2014).
28. M. Lahiri, R. Lapkiewicz, G. B. Lemos, A. Zeilinger, Theory of quantum imaging with undetected photons. *Phys. Rev. A* **92**, 013832 (2015).
29. P. Kwiat, H. Weinfurter, T. Herzog, A. Zeilinger, M. A. Kasevich, Interaction-free measurement. *Phys. Rev. Lett.* **74**, 4763–4766 (1995).
30. T. Rudolph, Better schemes for quantum interrogation in lossy experiments. *Phys. Rev. Lett.* **85**, 2925–2928 (2000).
31. R. F. Werner, Quantum states with Einstein-Podolsky-Rosen correlations admitting a hidden-variable model. *Phys. Rev. A* **40**, 4277–4281 (1989).
32. F. Ahnefeld, T. Theurer, D. Egloff, J. M. Matera, M. B. Plenio, Coherence as a Resource for Shor's Algorithm. *Phys. Rev. Lett.* **129**, 120501 (2022).
33. T. Vidick, S. Wehner, Does Ignorance of the Whole Imply Ignorance of the Parts? Large violations of noncontextuality in quantum theory. *Phys. Rev. Lett.* **107**, 030402 (2011).
34. M. Kewming, S. Shrapnel, A. White, J. Romero, Hiding ignorance using high dimensions. *Phys. Rev. Lett.* **124**, 250401 (2020).
35. A. Tavakoli, A. Hameedi, B. Marques, M. Bourennane, Quantum random access codes using single *d*-level systems. *Phys. Rev. Lett.* **114**, 170502 (2015).
36. A. Tavakoli, I. Herbauts, M. Żukowski, M. Bourennane, Secret sharing with a singled-level quantum system. *Phys. Rev. A* **92**, 030302 (2015).
37. A. Acín, N. Gisin, L. Masanes, From Bell's theorem to secure quantum key distribution. *Phys. Rev. Lett.* **97**, 120405 (2006).
38. N. Brunner, S. Pironio, A. Acin, N. Gisin, A. A. Méthot, V. Scarani, Testing the dimension of Hilbert spaces. *Phys. Rev. Lett.* **100**, 210503 (2008).
39. S. Wehner, M. Christandl, A. C. Doherty, Lower bound on the dimension of a quantum system given measured data. *Phys. Rev. A* **78**, 062112 (2008).
40. R. Gallego, N. Brunner, C. Hadley, A. Acín, Device-independent tests of classical and quantum dimensions. *Phys. Rev. Lett.* **105**, 230501 (2010).
41. O. Gühne, C. Budroni, A. Cabello, M. Kleinmann, J.-Å. Larsson, Bounding the quantum dimension with contextuality. *Phys. Rev. A* **89**, 062107 (2014).
42. M. Ray, N. G. Boddu, K. Bharti, L.-C. Kwek, A. Cabello, Graph-theoretic approach to dimension witnessing. *New J. Phys.* **23**, 033006 (2021).
43. S. Designolle, R. Uola, K. Luoma, N. Brunner, Set coherence: Basis-independent quantification of quantum coherence. *Phys. Rev. Lett.* **126**, 220404 (2021).
44. N. Brunner, M. Navascués, T. Vértesi, Dimension witnesses and quantum state discrimination. *Phys. Rev. Lett.* **110**, 150501 (2013).
45. V. Bargmann, Note on Wigner's theorem on symmetry operations. *J. Math. Phys.* **5**, 862–868 (1964).
46. M. Oszmaniec, D. J. Brod, E. F. Galvão, Measuring relational information between quantum states, and applications. arXiv:2109.10006 [quant-ph] (21 September 2021).
47. M. Navascues, K. F. Pál, T. Vértesi, M. Araújo, Self-testing in prepare-and-measure scenarios and a robust version of Wigner's theorem. arXiv:2306.00730 [quant-ph] (12 June 2023).
48. W. R. Clements, P. C. Humphreys, B. J. Metcalf, W. S. Kolthammer, I. A. Walmsley, Optimal design for universal multiport interferometers. *Optica* **3**, 1460 (2016).
49. A. Tavakoli, A. Pozas-Kerstjens, P. Brown, M. Araújo, Semidefinite programming relaxations for quantum correlations. arXiv:2307.02551 [quant-ph] (18 August 2023).
50. X. Li, D. Sun, K.-C. Toh, QSDPNAL: a two-phase augmented lagrangian method for convex quadratic semidefinite programming. *Mathem. Programm. Comput.* **10**, 703–743 (2018).
51. T. Giordani, R. Wagner, C. Esposito, A. Camillini, F. Hoch, G. Carvacho, C. Pentangelo, F. Ceccarelli, S. Piacentini, A. Crespi, N. Spagnolo, R. Osellame, E. F. Galvao, F. Sciarrino, *Code for "Experimental certification of contextuality, coherence and dimension in a programmable universal photonic processor"* (Zenodo, 2023); 10.5281/zenodo.8386354.
52. J. Eisert, D. Hangleiter, N. Walk, I. Roth, D. Markham, R. Parekh, U. Chabaud, E. Kashefi, Quantum certification and benchmarking. *Nat. Rev. Phys.* **2**, 382–390 (2020).
53. A. Ambainis, M. Banik, A. Chaturvedi, D. Kravchenko, A. Rai, Parity oblivious *d*-level random access codes and class of noncontextuality inequalities. *Quant. Inform. Process.* **18**, 1 (2019).
54. A. Chailloux, I. Kerenidis, S. Kundu, J. Sikora, Optimal bounds for parity-oblivious random access codes. *New J. Phys.* **18**, 045003 (2016).
55. M. Lostaglio, Certifying quantum signatures in thermodynamics and metrology via contextuality of quantum linear response. *Phys. Rev. Lett.* **125**, 230603 (2020).
56. M. Lostaglio, G. Senno, Contextual advantage for state-dependent cloning. *Quantum* **4**, 258 (2020).
57. K. Flatt, H. Lee, C. R. I. Carceller, J. B. Brask, J. Bae, Contextual advantages and certification for maximum-confidence discrimination. *PRX Quantum* **3**, 030337 (2022).
58. C. R. Carceller, K. Flatt, H. Lee, J. Bae, J. B. Brask, Quantum vs noncontextual semi-device-independent randomness certification. *Phys. Rev. Lett.* **129**, 050501 (2022).
59. M. D. Mazurek, M. F. Pusey, R. Kunjwal, K. J. Resch, R. W. Spekkens, An experimental test of noncontextuality without unphysical idealizations. *Communications* **7**, 11780 (2016).
60. M. D. Mazurek, M. F. Pusey, K. J. Resch, R. W. Spekkens, Experimentally bounding deviations from quantum theory in the landscape of generalized probabilistic theories. *PRX Quantum* **2**, 020302 (2021).
61. X. Zhan, E. G. Cavalcanti, J. Li, Z. Bian, Y. Zhang, H. M. Wiseman, P. Xue, Experimental generalized contextuality with single-photon qubits. *Optica* **4**, 966 (2017).
62. Q. Zhang, C. Zhu, Y. Wang, L. Ding, T. Shi, X. Zhang, S. Zhang, W. Zhang, Experimental test of contextuality based on state discrimination with a single qubit. *Chin Phys Lett* **39**, 080301 (2022).
63. R. D. Baldijão, R. Wagner, C. Duarte, B. Amaral, M. T. Cunha, Emergence of noncontextuality under quantum darwinism. *PRX Quantum* **2**, 030351 (2021).
64. V. J. Wright, M. Farkas, An invertible map between Bell non-local and contextuality scenarios. arXiv:2211.12550 [quant-ph] (22 November 2022).
65. J. H. Selby, D. Schmid, E. Wolfe, A. B. Sainz, R. Kunjwal, R. W. Spekkens, Accessible fragments of generalized probabilistic theories, cone equivalence, and applications to witnessing nonclassicality. *Phys. Rev. A* **107**, 062203 (2023).
66. J. H. Selby, E. Wolfe, D. Schmid, A. B. Sainz, An open-source linear program for testing nonclassicality. arXiv:2204.11905 [quant-ph] (25 April 2022).
67. V. P. Rossi, D. Schmid, J. H. Selby, A. B. Sainz, Contextuality with vanishing coherence and maximal robustness to dephasing. *Phys. Rev. A* **108**, 032213 (2023).
68. N. Harrigan, R. W. Spekkens, Einstein, incompleteness, and the epistemic view of quantum states. *Found Phys* **40**, 125–157 (2010).
69. D. Schmid, J. H. Selby, R. W. Spekkens, Addressing some common objections to generalized noncontextuality. arXiv:2302.07282 [quant-ph] (14 February 2023).
70. D. Schmid, R. W. Spekkens, E. Wolfe, All the noncontextuality inequalities for arbitrary prepare-and-measure experiments with respect to any fixed set of operational equivalences. *Phys. Rev. A* **97**, 062103 (2018).
71. A. Tavakoli, E. Z. Cruzeiro, R. Uola, A. A. Abbott, Bounding and simulating contextual correlations in quantum theory. *PRX Quantum* **2**, 020334 (2021).
72. A. Chaturvedi, M. Farkas, V. J. Wright, Characterising and bounding the set of quantum behaviours in contextuality scenarios. *Quantum* **5**, 484 (2021).
73. D. Schmid, J. H. Selby, E. Wolfe, R. Kunjwal, R. W. Spekkens, Characterization of noncontextuality in the framework of generalized probabilistic theories. *PRX Quantum* **2**, 010331 (2021).
74. F. Shahandeh, Contextuality of general probabilistic theories. *PRX Quantum* **2**, 010330 (2021).
75. L. Hardy, Quantum theory from five reasonable axioms. arXiv:0101012 [quant-ph] (25 September 2001).
76. J. Barrett, Information processing in generalized probabilistic theories. *Phys. Rev. A* **75**, 032304 (2007).
77. M. Müller, Probabilistic theories and reconstructions of quantum theory. *SciPost Phys. Lect. Notes* 28 (2021).
78. M. Plávala, General probabilistic theories: An introduction. *Phys. Rep.* **1033**, 1–64 (2023).
79. V. Gitton, M. P. Woods, Solvable criterion for the contextuality of any prepare-and-measure scenario. *Quantum* **6**, 732 (2022).
80. A. Arriola, S. Gross, N. Jovanovic, N. Charles, P. G. Tuthill, S. M. Olaizola, A. Fuerbach, M. J. Withford, Low bend loss waveguides enable compact, efficient 3D photonic chips. *Opt. Express* **21**, 2978–2986 (2013).
81. G. Corrielli, S. Atzeni, S. Piacentini, I. Pitsios, A. Crespi, R. Osellame, Symmetric polarization-insensitive directional couplers fabricated by femtosecond laser writing. *Opt. Express* **26**, 15101–15109 (2018).
82. F. Ceccarelli, S. Atzeni, A. Prencipe, R. Farinaro, R. Osellame, Thermal phase shifters for femtosecond laser written photonic integrated circuits. *J Lightw. Technol.* **37**, 4275–4281 (2019).
83. F. Ceccarelli, S. Atzeni, C. Pentangelo, F. Pellegatta, A. Crespi, R. Osellame, Low power reconfigurability and reduced crosstalk in integrated photonic circuits fabricated by femtosecond laser micromachining. *Laser Photon. Rev.* **14**, 2000024 (2020).
84. C. Alexiev, J. C. C. Mak, W. D. Sacher, J. K. S. Poon, Calibrating rectangular interferometer meshes with external photodetectors. *OSA Continuum* **4**, 2892 (2021).

85. J. Carolan, C. Harrold, C. Sparrow, E. Martn-Lpez, N. J. Russell, J. W. Silverstone, P. J. Shadbolt, N. Matsuda, M. Oguma, M. Itoh, G. D. Marshall, M. G. Thompson, J. C. F. Matthews, T. Hashimoto, J. L. O'Brien, A. Laing, Universal linear optics. *Science* **349**, 711–716 (2015).
86. N. C. Harris, G. R. Steinbrecher, M. Prabhu, Y. Lahini, J. Mower, D. Bunandar, C. Chen, F. N. Wong, T. Baehr-Jones, M. Hochberg, Quantum transport simulations in a programmable nanophotonic processor. *Nat. Photon.* **11**, 447–452 (2017).
87. M. Pont, R. Albiero, S. E. Thomas, N. Spagnolo, F. Ceccarelli, G. Corrielli, A. Brieussel, N. Somaschi, H. Huet, A. Harouri, A. Lemaitre, I. Sagnes, N. Belabas, F. Sciarrino, R. Osellame, P. Senellart, A. Crespi, Quantifyingn-Photon indistinguishability with a cyclic integrated interferometer. *Phys. Rev. X* **12**, 031033 (2022).
88. F. Hoch, T. Giordani, N. Spagnolo, A. Crespi, R. Osellame, F. Sciarrino, Characterization of multimode linear optical networks. *Adv. Photon. Nexus* **2**, 016007 (2023).

Acknowledgments: We would like to thank E. Zambrini, V. P. Rossi, A. Te'eni, and A. Ruiz-Molero for fruitful discussions. The programmable UPP was partially fabricated at PoliFAB, the micro- and nanofabrication facility of Politecnico di Milano (at www.polifab.polimi.it/). C.P., F.C., and R. O. wish to thank the PoliFAB staff for the valuable technical support. **Funding:** R.W. and A.Ca. acknowledge support from FCT–Fundação para a Ciência e a Tecnologia (Portugal) through PhD grants SFRH/BD/151199/2021 and SFRH/BD/151190/2021. E.F.G. acknowledges support from FCT–Fundação para a Ciência e a Tecnologia (Portugal) via project CEECINST/00062/2018. We acknowledge support from the ERC Advanced Grant QU-BOSS (QUantum advantage via nonlinear BOSon Sampling, grant agreement no. 884676) and from PNRR MUR project PE0000023-NQSTI (Spoke 4 and Spoke 7). This work is also supported by Horizon Europe project FoQaCiA, grant agreement no. 101070558. **Author contributions:** T.G., C.E., F.H., G.C., N.S., F.S., R.W., A.Ca., and E.F.G. conceived the concept and experiment. R.W., A.Ca., and E.F.G. developed the theory of the method. C.P., F.C., S.P., A.Cr., and R.O. fabricated the photonic chips and characterized the integrated device using classical optics. C.E., T.G., F.H., G.C., N.S., and F.S. carried out the quantum experiments and performed the data analysis. All the authors discussed the results and contributed to the writing of the paper. **Competing interests:** F.C. and R.O. are cofounders of the company Ephos. The authors declare that they have no other competing interests. **Data and materials availability:** All data needed to evaluate the conclusions in the paper are present in the paper and/or the Supplementary Materials or in the repository at https://zenodo.org/record/8386354.

Submitted 26 June 2023
Accepted 2 October 2023
Published 3 November 2023
10.1126/sciadv.adj4249